



## Synthesis of (100) surface oriented MIL-88A-Fe with rod-like structure and its enhanced fenton-like performance for phenol removal

Xiaoyuan Liao<sup>a,b,\*</sup>, Fan Wang<sup>a</sup>, Fang Wang<sup>c</sup>, Yi Cai<sup>a</sup>, Yue Yao<sup>a,b,\*</sup>, Bo-Tao Teng<sup>c</sup>, Qinglan Hao<sup>a,b</sup>, Shuxiang Lu<sup>a,b,\*</sup>



<sup>a</sup> College of Chemical Engineering and Materials Science, Tianjin University of Science and Technology, Tianjin 300457, China

<sup>b</sup> Tianjin Key Laboratory of Brine Chemical Engineering and Resource Eco-utilization, China

<sup>c</sup> Key Laboratory of the Ministry of Education for Advanced Catalysis Materials, College of Chemistry and Life Sciences, Zhejiang Normal University, Jinhua, Zhejiang, 321004, China

### ARTICLE INFO

**Keywords:**  
MIL-88A-Fe  
Fenton-like catalysts  
Morphology  
Exposed (100) surface

### ABSTRACT

Morphology of MIL-88A-Fe greatly affects their Fenton-like performance. In this work, rod-like, spindle-like and diamond-like MIL-88A-Fe was prepared by changing the ratio of solvents in solvothermal process. Their physicochemical properties are fully investigated by XRD, SEM, TEM, XPS, ESR, and DFT calculation, which confirmed that the exposed (100) ratio of MIL-88A-Fe determined its catalytic performance. The (100) surface of MIL-88A-Fe showed lower energy barrier for H<sub>2</sub>O<sub>2</sub> dissociated into ·OH (dissociated energy 0.58 eV), corresponding value is 0.8 eV for (101) surface. The Fenton-like performance has the order of r-MIL-88A (TOF 5.0 h<sup>-1</sup>) > s-MIL-88A (TOF 3.3 h<sup>-1</sup>) > d-MIL-88A (TOF 2.5 h<sup>-1</sup>), when r-MIL-88A used as catalyst, phenol could be removed 100% in 15 min by the help of H<sub>2</sub>O<sub>2</sub> at room conditions, its activity are better than that of reported Fe-based MOFs, such as MIL-88B-Fe, MIL-101-Fe, and MIL-53(Fe) etc. This finding probably provide a Fenton-like catalyst by choosing the suitable crystal phase of Fe-based metal organic framework.

### 1. Introduction

Waste water from industry contains a wide range of toxic organic compounds, such as phenol, which is harmful to environment and human health. The effective treatment of waste water is sustainable development to environment. Advanced oxidation processes (AOPs), as highly effective and promising technologies, have been extensively utilized in the removal of various hazardous organic pollutants in waste water [1]. Nevertheless, for traditional homogeneous Fenton reaction, there are some inherent drawbacks: Fe containing sludge production, and unrecoverable catalyst. To overcome above problems, heterogeneous Fenton-like reaction using insoluble solid catalysts has been developed. Various iron-based catalysts, such as iron-oxygen compounds [2], and Fe immobilized materials [3], have been used in AOP reaction. Unfortunately, this catalyst is easily deactivated for iron leaching or low activity [4,5]. Accordingly, the development of new types of heterogeneous catalysts with high activity and good stability is highly desired.

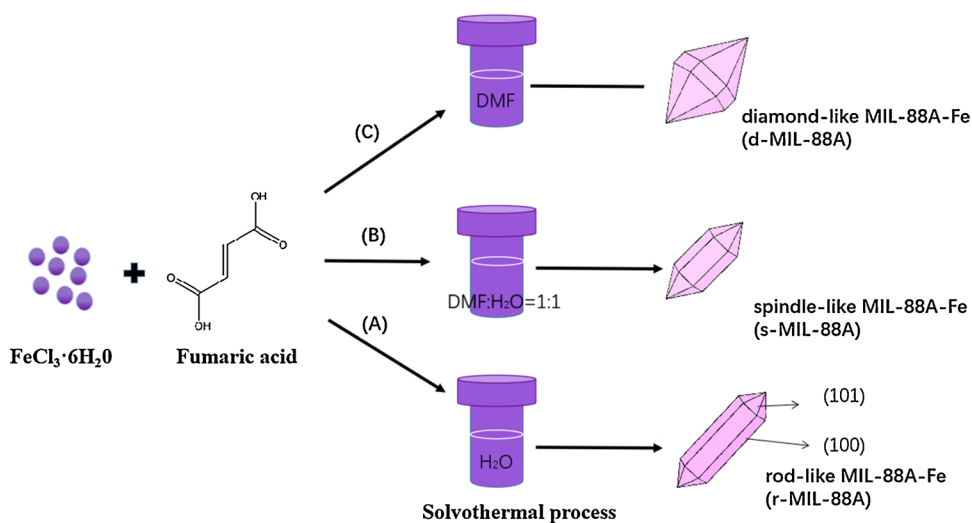
Over the past decade, as a multifunctional porous materials, metal organic frameworks (MOFs) are crystalline organic-inorganic hybrids composites. MOFs exhibit excellent characteristic features, such as well-

defined structure, large pore volume and high specific areal, and have received substantial attention in applications in the area of adsorption [6–8] photo-catalysis [9–15] and catalysis [16–18]. Fe-based MOFs, a heterogeneous Fenton-like materials, have been widely used in environmental remediation, especially for phenol removal [1,19–22]. Fe-based MOFs, including MIL-88A-Fe, MIL-88B-Fe, MIL-53-Fe, MIL-100-Fe and MIL-101-Fe etc [23]. Among of them, the MIL-88A-Fe is the most active one. This material is a 3D framework built-up from trimers of Fe<sup>III</sup> octahedral linked to fumarate dianions [24], exhibits excellent chemical/water stability and is relatively easy synthesis [25,26] and good swelling character [27]. The existence of coordinatively unsaturated iron sites of trimeric Fe<sub>3</sub>·μ<sub>3</sub>-oxo cluster in MIL-88A-Fe allows strong interactions with H<sub>2</sub>O<sub>2</sub>, resulting in the high-efficiently activate H<sub>2</sub>O<sub>2</sub> [28,29]. Recently, many works reported the MIL-88A-Fe used for organic pollutants removal [30–32].

Indeed, owing to MOFs are structurally adaptive [33], it is reported that the Fenton-like activity of Fe-Co MOF are strongly affected by the shape of the nanocrystals [34]. Even if similar Fe-based MOFs, such as MIL-88B-Fe and MIL-101-Fe, owned identical chemical compositions but different exposed facets or shapes, the activity of the former is about 5 times than that of the later ( $k = 8.15 \times 10^{-3}$  vs  $1.54 \times 10^{-3}$ ) [20].

\* Corresponding authors at: College of Chemical Engineering and Materials Science, Tianjin University of Science and Technology, Tianjin 300457, China.

E-mail addresses: [liaoxy@tust.edu.cn](mailto:liaoxy@tust.edu.cn) (X. Liao), [yueyao@tust.edu.cn](mailto:yueyao@tust.edu.cn) (Y. Yao), [lsx@tust.edu.cn](mailto:lsx@tust.edu.cn) (L. Shuxiang).



**Scheme 1.** Schematic illustration of the formation process of shape-controlled MIL-88A-Fe; three kinds of morphologies, and their corresponding nomenclature.

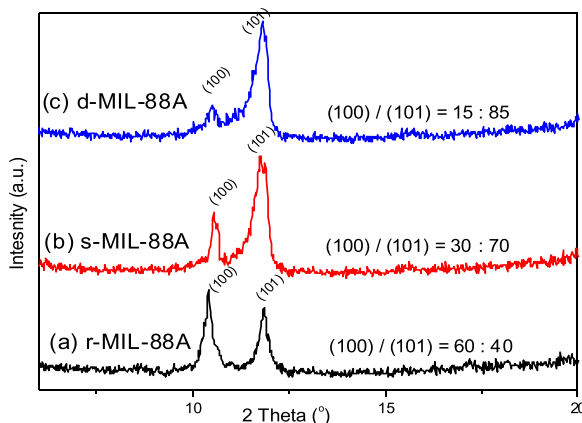


**Fig. 1.** XRD patterns of shape-controlled MIL-88A-Fe.

As for MIL-88A-Fe material, though many works confirmed it performed good Fenton-like activity, MIL-88A-Fe presented in these works were amorphous or prism-like [17,18]. In fact, MIL-88A-Fe has at least three kind crystallographic structure, such as rod-like, spindle-like and diamond-like structure [35]. Exposed Fe sites were intrinsically determined by the crystallographic structure, orientations, and nanostuctures of catalysts [36–38]. Different shaped MIL-88A-Fe would perform different catalytic activity. Through some studies have reported that Fe-based MOFs used for environmental remediation, it still remains unclear in the following two aspects: (1) The dissociated pathway of  $\text{H}_2\text{O}_2$  over the MIL-88A-Fe surface are not unclear; (2) The reason of the MOF facet-dependent catalytic activities has not been explored.

In this study, shape-controlled MIL-88A-Fe nanocrystals with different oriented facets were synthesized by solvent mediated method, and employed as Fenton-like catalysts for phenol removal. The physicochemical properties of MIL-88A-Fe nanocrystals were characterized, the interaction between  $\text{H}_2\text{O}_2$  and its surfaces was investigated by DFT calculation. Our results showed that the MIL-88A-Fe with preferentially exposed (100) surface, performed lower energy barrier for  $\text{H}_2\text{O}_2$  dissociating into ·OH, which determine the Fenton-like activity. This study is the first investigation to utilize shaped MIL-88A-Fe as catalysts for organic contamination removal, and provides a new system for removal of phenol in water and boosts the mechanistic innovations in  $\text{H}_2\text{O}_2$ -Fenton reaction over surfaces of MIL-88A-Fe.

## 2. Experimental

### 2.1. Catalyst preparation

Shape-controlled MIL-88A-Fe was prepared according to Scheme 1. Specifically, 1.352 g  $\text{FeCl}_3 \cdot 6\text{H}_2\text{O}$  and 0.580 g fumaric acid were dissolved in different ratio of water/DMF( $\text{N,N}$ -dimethylformamide). The mixture was transferred into a Teflon reaction kettle, placed in an autoclave, and heated to 65 °C for 4 h. Finally, the raw product was washed by DMF/deionized water for four times, and dried at 60 °C. The three kinds of MIL-88A-Fe, i.e., rod-like, spindle-like and diamond-like, are denoted as r-MIL-88A, s-MIL-88A, d-MIL-88A, respectively (Scheme 1). The water/DMF ratio is at a high level, the synthesized crystal shows a (100) orientation. Increasing the water/DMF ratio to 1:1, and pure DMF (Scheme 1), the crystal layer of the (101) orientation grows favorably.

### 2.2. Computational details

Spin-polarization calculations were performed using Vienna ab initio simulation package (VASP) code based on density functional theory. The Perdew-Burke- Ernzerhof (PBE) functional was adopted to treat the electron exchange and correlation effects by the generalized gradient approximation (GGA). Transition states (TS) of  $\text{H}_2\text{O}_2$  desorption and diffusion were calculated with the climbing image nudged elastic band (CINEB) method. The activation barrier was defined as the total energy difference between the transition state and the corresponding stable structures of reactants or products. Frequency analysis was carried out to verify no imaginary frequency for the stable configurations and a single imaginary one for the transition state structure.

### 2.3. Characterization

XRD (X-ray powder diffraction) data were acquired on Bruker AXS D8-Focus diffractometer using  $\text{Cu K}\alpha$  radiation. The data were collected from in a  $2\theta$  range of 5 to 40° with a scanning speed of 5°/min. Brunauer-Emmett-Teller (BET) surface areas were gotten on ASAP 2020 plus HD88. SEM (Scanning electronic microscopy) images were taken with Hitachi FESEM-4800. The transmission electron microscopy (TEM) images were obtained by using a TECNAI G2 F20 instrument. XPS spectra were performed on a PHI 550 ESCA/SAM high performance electron spectrometer equipped with monochromatized Al K X-ray source ( $\hbar = 1486.6$  eV). The C1s peak (284.6 eV) was used for the calibration of binding energy values. Electron Spin Resonance (ESR)

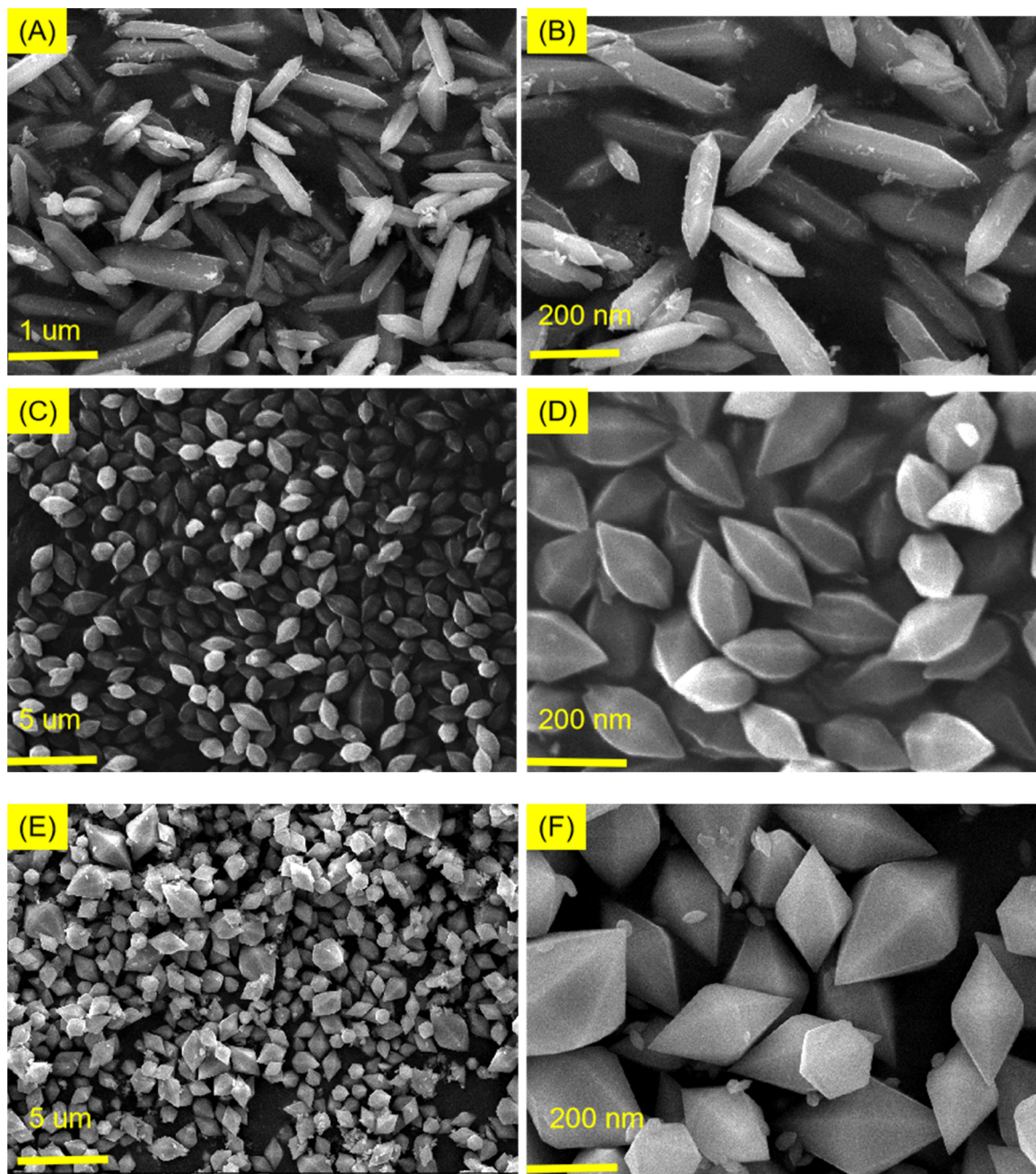


**Fig. 2.** SEM images: r-MIL-88A (A, B); s-MIL-88A (C,D); d-MIL-88A (E,F).

experiments were performed on a Bruker A300 spectrometer (Germany) with DMPO as spin-trapping agent. The reactive oxygen species ( $\cdot\text{OH}$  and  $\cdot\text{O}_2^-$ ) can test by the a fluorescence method proposed in ref. [39]

#### 2.4. Phenol removal experimental method and products analysis

In a typical experiment, the degradation experiments were carried out in a three-necked flask (250 mL). Catalyst was dispersed in phenol solution by sonication for 5 min. Then the degradation reaction was initiated by adding  $\text{H}_2\text{O}_2$  under magnetic stirring. The solution was sampled periodically and analyzed by Agilent Technologies 1260 Infinity Liquid Chromatography equipped with C18 column (250 × 4.6 mm). Phenol removal rate was calculated as follows: phenol removal rate =  $(\text{C}_0 - \text{C})/\text{C}_0$ ,  $\text{C}_0$  = initial concentrations of phenol solution,  $\text{C}$  = the concentration of phenol solution after degradation [40].

Each degradation experiment was test three times and the given data are arithmetic means of three measured results.

### 3. Results and discussion

#### 3.1. XRD, SEM and TEM

The crystalline structure of MIL-88A-Fe was analyzed and shown in Fig. 1, it is seen that the synthesis solution, the ratio of water/DMF, can significantly affect the PXRD pattern and crystallinity. The XRD patterns of MIL-88A-Fe show the presence of (100) (at 10.2°) and (101) (at 11.8°) [41]. The synthesis solution has a certain function in controlling the MIL-88A-Fe crystal orientation. The orientation of MIL-88A-Fe crystal transits from (100) to (101) with increasing amount of DMF. From the peak area of XRD, and the (100) surface occupy the ratio of 60%, 30% and 15%, for r-MIL-88A, s-MIL-88A, d-MIL-88A,

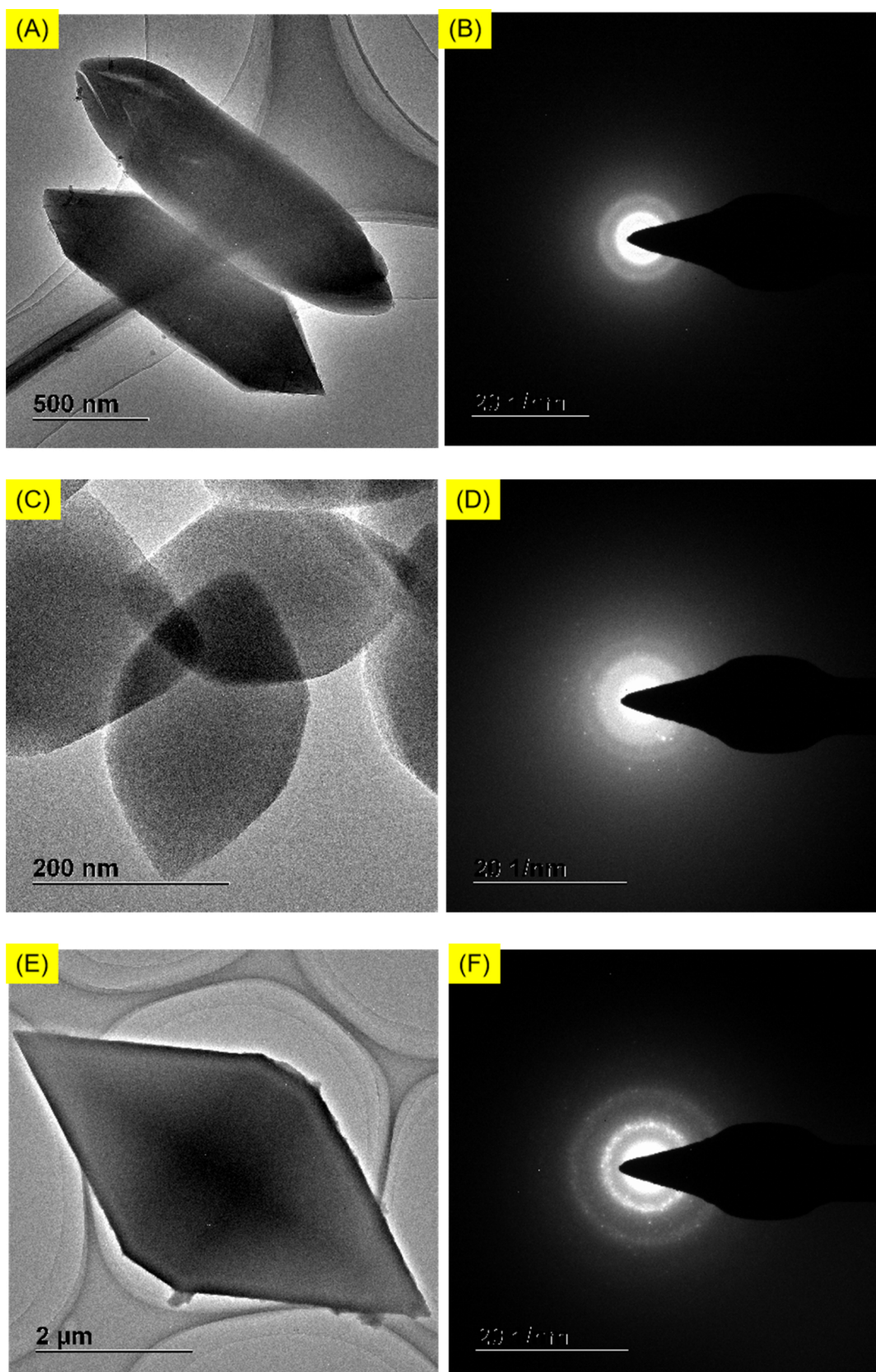


Fig. 3. TEM images: r-MIL-88A (A, B); s-MIL-88A (C,D); d-MIL-88A (E,F) (left column TEM; right column SAED).

**Table 1**  
Physicochemical properties of MIL-88A.

| Catalyst  | $S_{BET}$ ( $m^2/g$ ) | $V_p$ ( $cm^3/g$ ) | D (nm) |
|-----------|-----------------------|--------------------|--------|
| r-MIL-88A | 24.3                  | 0.065              | 10.7   |
| s-MIL-88A | 20.7                  | 0.046              | 10.6   |
| d-MIL-88A | 12.0                  | 0.032              | 8.8    |

respectively.

The nucleation rate of MOF determines its morphology or particle size. Generally, fast nucleation produces a larger amount nuclei, and shortens the crystal growth stage, leading to small-sized particles. On the contrary, slow nucleation produces large-sized particles [42]. The solvation greatly effect nucleation speed of MOF. In this prepared process of MIL-88A-Fe, when use DMF as solvent, for its strong polarity value ( $\mu = 3.86$  D), DMF greatly slowed down the generation speed of MIL-88A-Fe crystals, leading to large-sized d-MIL-88A crystals [43,44]. However, when water ( $\mu = 1.85$  D) as solvent, the nucleation quickly proceeded to generate small-sized r-MIL-88A. For middle-sized s-MIL-88A, the middle-sized particle appeared due to middle crystallization speed.

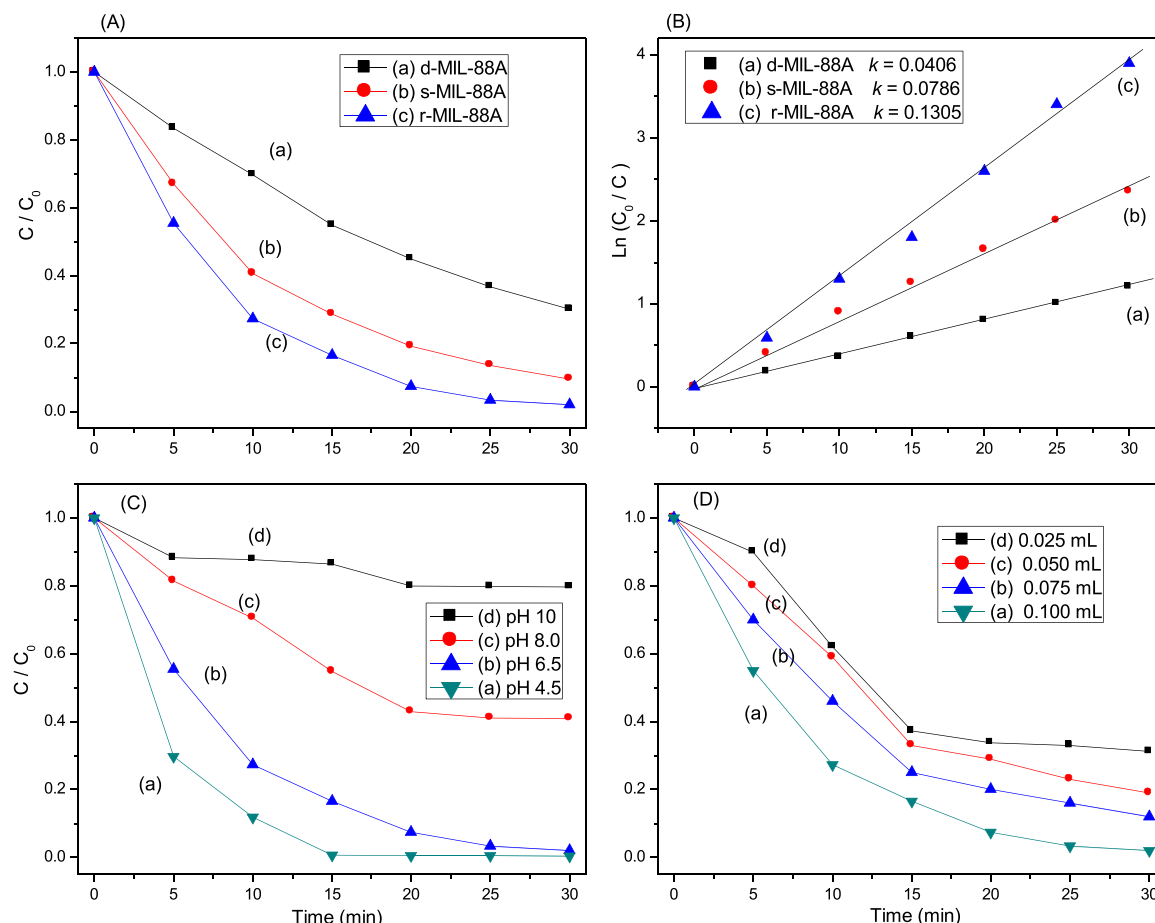
As revealed in the SEM images displayed in Fig. 2, the MIL-88A with different morphology were successfully prepared via the adopted hydrothermal methods. It can be seen that r-MIL-88A is made up of rod-shaped structure with 100–300 nm length (Fig. 2A,B). Fig. 2C,D shows that s-MIL-88A is composed of spindle-like structure. As for d-MIL-88A (Fig. 2E,F), it is made up of diamond-like structure. This character make our investigations on the relationship of performance and specific morphology possible.

The surface morphology and microstructure of the samples have been carefully investigated by TEM (Fig. 3, left column) coupled with selected area electron diffraction (SAED) (Fig. 3, right column), which provides a convincing explanation on the variation of morphology. As shown in Fig. 3 A,C,E, confirms the three kind morphology of MIL-88A. The SAED image (Fig. 3 B,D,F) reveal that the surface of MIL-88A is dominated by (100) and (101) crystal faces. The (100) surface occupied ratio has the order of r-MIL-88A > s-MIL-88A > d-MIL-88A

In summary, this three samples all have the (100) and (101) facets. With variation in terms of exposed facets, the MIL-88A-Fe samples should be different in chemical property, and hence exhibit distinct catalytic performance.

### 3.2. BET

Table 1 give the BET specific surface area of r-, s-, d-MIL-88A, are 24.3, 20.7, 12.0  $m^2/g$ , respectively. MIL-88A-Fe samples show a very small specific surface area, which is similar to Mn-based MOF materials [45,46]. From Fig. S1, the hysteresis loops in the isotherm curves are observed, and can be ascribed to typical type IV isotherm with H3 hysteresis loop [47], means that presence of mesopores in the range from 3 to 14 nm (Fig. S2). From r-MIL-88A to d-MIL-88A, the hysteresis loop is narrowing, which means the pore size distribution is narrow. It could be seen from Fig. S3, and r-MIL-88A have microporous structure (0.9 nm) and mesopores structure (4–16 nm). Table 1, show that, from r-MIL-88A to d-MIL-88A, the pore volume and size both decrease (Table 1).

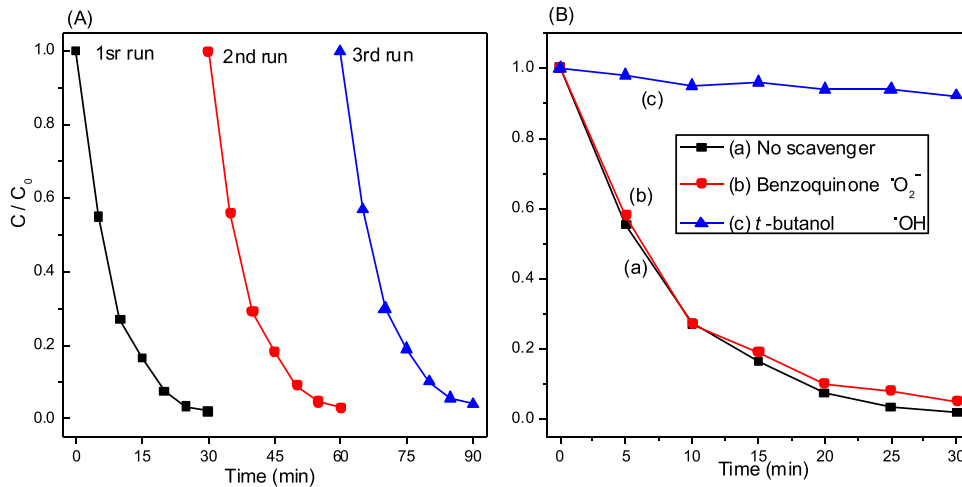


**Fig. 4.** (A) Catalytic performance for over different shaped MIL-88A-Fe (Reaction conditions: phenol 150 ml (100 ppmw);  $H_2O_2$ , 0.10 mL, cat. 0.015 g, 20 °C); (B) degradation efficiency of shaped MIL-88A-Fe; (C) the effluence of pH values; (D) the effluence of  $H_2O_2$  load.

**Table 2**

Compared with published works for Fenton-like phenol degradation with Fe-based MOFs.

| Entry | Catalysts                      | Reaction conditions |   |                       |                    | Degradation performance | Ref.      |
|-------|--------------------------------|---------------------|---|-----------------------|--------------------|-------------------------|-----------|
|       |                                | Temperature(°C)     | [H <sub>2</sub> O <sub>2</sub> ]/phenol | Load of catalyst(g/L) | Reaction time(min) |                         |           |
| 1     | r-MIL-88A                      | 20                  | 2.5:1                                   | 0.1                   | 20                 | 93%                     | This work |
| 2     | r-MIL-88A                      | 20                  | 5:1                                     | 0.1                   | 15                 | 100%                    | This work |
| 3     | s-MIL-88A                      | 20                  | 2.5:1                                   | 0.1                   | 20                 | 81%                     | This work |
| 4     | d-MIL-88A                      | 20                  | 2.5:1                                   | 0.1                   | 20                 | 65%                     | This work |
| 5     | MIL-88B                        | 20                  | 10:1                                    | 0.1                   | 20                 | ~90%                    | [20]      |
| 6     | Fe <sub>3</sub> O <sub>4</sub> | 20                  | 10:1                                    | 0.1                   | 20                 | ~12%                    | [20]      |
| 7     | MIL-101-Fe                     | 20                  | 10:1                                    | 0.1                   | 20                 | ~22%                    | [20]      |
| 8     | MIL-53(Fe)                     | 20                  | 10:1                                    | 1.17                  | 20                 | 5% <                    | [20]      |
| 9     | MIL-53(Fe)                     | 35                  | 14:1                                    | 1.17                  | 60                 | ~99%                    | [49]      |
| 10    | Fe(BDC)                        | 35                  | 14:1                                    | 1.17                  | 60                 | ~92%                    | [49]      |
| 11    | NH <sub>2</sub> -MIL-53(Fe)    | 35                  | 14:1                                    | 0.1                   | 60                 | ~90%                    | [50]      |

**Fig. 5.** (A) Reusability of r-MIL-88A; (B) The effect of scavengers. (Reaction conditions: phenol 150 ml (100 ppmw); H<sub>2</sub>O<sub>2</sub>, 0.10 mL, cat. 0.015 g, 20 °C).

### 3.3. Catalytic activity

To deeper understand the morphology-dependent Fenton-like catalytic activity, the polyhedral r-MIL-88A, s-MIL-88A, d-MIL-88A samples were employed for phenol degradation. It can be obtained from Fig. 4A that the r-MIL-88A reveals the fastest degradation, and the degradation degree reaches about 100% in 25 min at mild reaction conditions. The d-MIL-88A displays the worst degradation rate about 38% in 25 min. The degradation of phenol can be regarded as a pseudo-first order reaction, and the reaction kinetics can be expressed as follows:  $\ln(C_0/C) = k_a t$ , where  $k_a$  is the degradation rate constant [48],  $C_0$  and  $C$  are the initial concentration and the concentration at a reaction time  $t$ , respectively. From the kinetic curves in Fig. 4B, the degradation rate constant can be calculated as the order: r-MIL-88A ( $k_a = 0.1305$ ) > s-MIL-88A ( $k_a = 0.0786$ ) > d-MIL-88A ( $k_a = 0.0406$ ).

Fig. 4C shows the catalytic degradation of phenol by r-MIL-88A at various pH values. The phenol could be quickly removed when pH is below 6.5. When pH is higher than 10, the activity is significantly decreased. At the investigated pH values range, the best catalytic activity toward phenol degradation can be found at pH 4.5. Fig. 4D shows the optimization of H<sub>2</sub>O<sub>2</sub> load. When H<sub>2</sub>O<sub>2</sub> increasing in the reaction system, the catalytic activity is increasing obviously. When the 0.1 mL H<sub>2</sub>O<sub>2</sub> was added into the reaction system, the phenol removal was found to near 100% after in 15 min. It can be deduced that the amount of H<sub>2</sub>O<sub>2</sub> is a positive influential parameter for phenol removal.

The optimal phenol removal conditions could be summarized: phenol 150 mL (100 ppmw), 0.015 g r-MIL-88A as catalyst, reaction time 15 min, H<sub>2</sub>O<sub>2</sub> 0.20 mL, 20 °C.

It is interesting to compare the degradation phenol activity for

different shaped MIL-88A with published sister catalysts. Table 2 shows clearly r-MIL-88A perform the best activity, as compared with the available results. For the MIL-88A composites, the r-MIL-88A is most active, and the d-MIL-88A least. These differences can be attributed to the change of shape. As shown in Table 1, compared with published catalysts, r-MIL-88A performs the best activity, and phenol degradation reach as high as 100% in 15 min (Entry 2), with the catalyst load of 0.1 g/L, and the ratio of [H<sub>2</sub>O<sub>2</sub>]/phenol is 5:1, at 20 °C. For MIL-88B, when performing ~90% phenol degradation at 20 °C, it needs very a large number of H<sub>2</sub>O<sub>2</sub> ([H<sub>2</sub>O<sub>2</sub>]/phenol = 10). And at same conditions, Fe<sub>3</sub>O<sub>4</sub> has slight acclivity (~12% removal performance). For other Fe-based MOF, such as MIL-53(Fe) or Fe(BDC), they need higher reaction temperature (35 °C), longer reaction time (60 min). This comparison gives us the confidence that our catalysts have higher activity.

Repeatability performance of a catalyst is very important for practical application. As shown in Fig. 5A. The r-MIL-88A catalyst exhibited a slight decline which was approximately 3% after at least three times recycling, indicating its high repeatability.

### 3.4. XPS

X-ray photoelectron spectroscopy (XPS) was used to determine the chemical information over the surfaces of the three kinds of MIL-88A-Fe. In Fig. 6A, the XPS survey spectrum indicate the existence of Fe, C and O elements. C1s spectrum of r-MIL-88A, given in Fig. 6B, the appearance of two peaks at 288.2, and 284.3 eV could be ascribed to carboxylic bonds and benzoic rings of r-MIL-88A [51–53] respectively. Fig. 6C displays the high-resolution XPS spectra of O1s, three peaks at binding energies of 531.6 eV, 531.0 eV and 530.4 eV are ascribed to

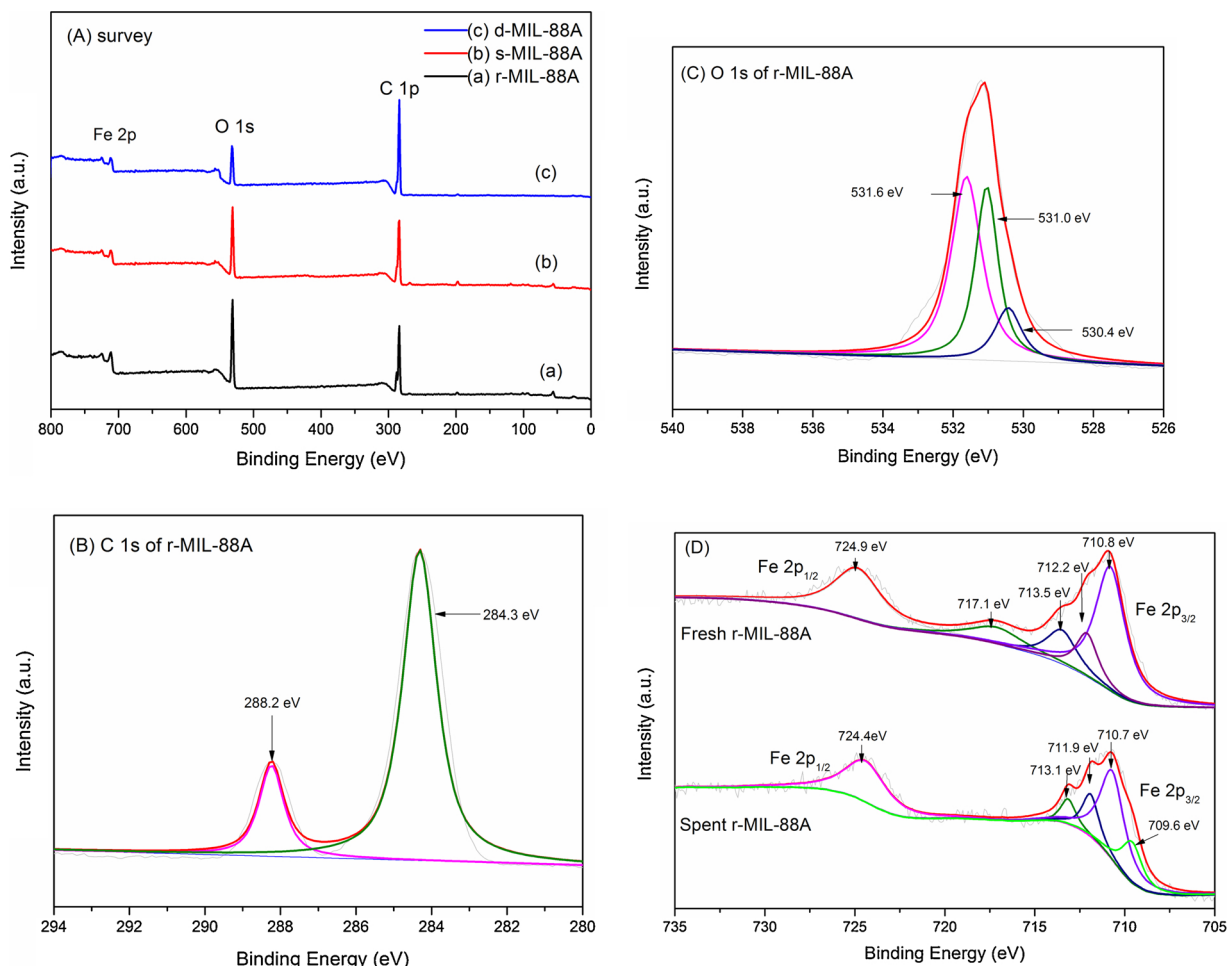


Fig. 6. XPS spectra of MIL-88A-Fe.

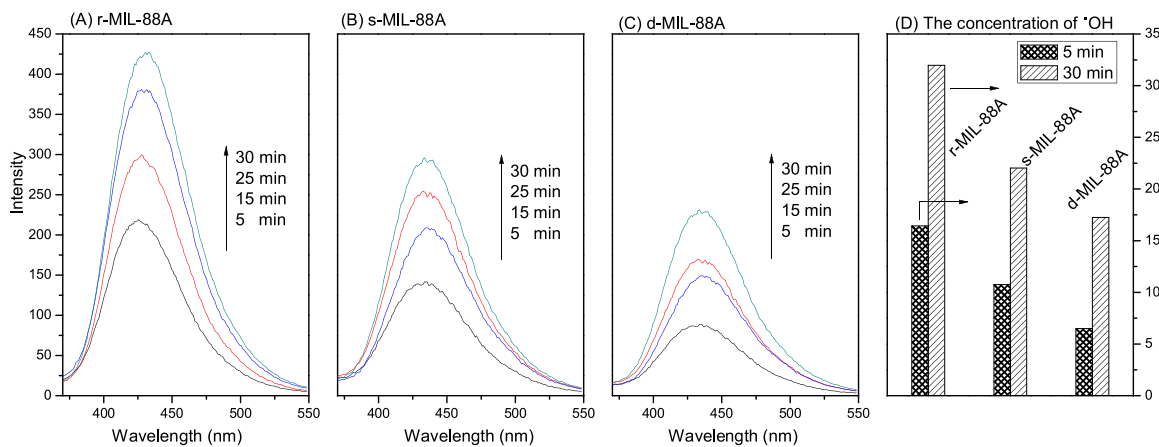
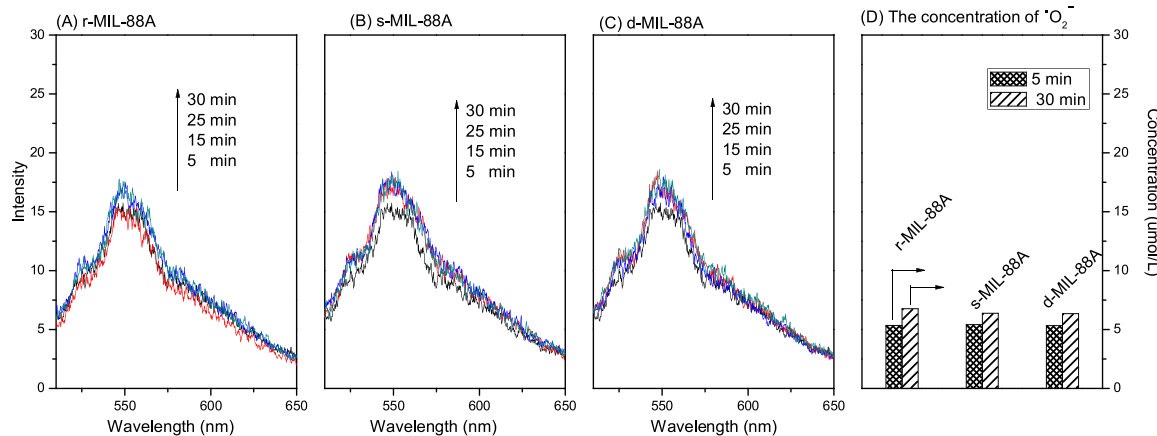


Fig. 7. The fluorescence emission spectra of terephthalic acid (TA)-·OH adducts at an initial ultrapure water (A–C), and the concentration of ·OH (D).

C–O, the oxygen components on the carboxylate groups and the Fe–O bonds of r-MIL-88A, respectively [54–56].

As shown in Fig. 6D, the binding energy peak at 710.8 eV and 724.9 eV could assign to the Fe 2p<sub>3/2</sub>, and Fe 2p<sub>1/2</sub>, respectively [57,58], and the peak distance was about 14.1 eV. The two peaks with a satellite signal at 717.1 eV are feature of Fe<sup>III</sup> in r-MIL-88A structure [59]. Fe2p<sub>3/2</sub> peak of fresh s-MIL-88A could be fitted into three

contributions at 713.5, 712.2, and 710.8 eV, respectively, indicating that only Fe<sup>III</sup> existed on fresh r-MIL-88A [15]. After interaction with H<sub>2</sub>O<sub>2</sub>, in comparison with the Fe<sup>III</sup> typical peaks of the r-MIL-88A has shifted to low binding energy. As shown Fig. 4(D), deconvolution of the Fe2p<sub>3/2</sub> peak of H<sub>2</sub>O<sub>2</sub> treated s-MIL-88A showed that Fe<sup>II</sup> appeared on s-MIL-88A, and the satellite signal at 717.1 eV is disappear, which can be attributed to an H<sub>2</sub>O<sub>2</sub> interfacial contact r-MIL-88A, indicating that



**Fig. 8.** The fluorescence emission spectra of NBD-Cl- $\cdot\text{O}_2^-$  adducts at an initial ultrapure water(A–C), and the concentration of  $\cdot\text{O}_2^-$  (D).

some  $\text{Fe}^{\text{III}}$  was reduced to  $\text{Fe}^{\text{II}}$  during the Fenton-like reaction.

### 3.5. Reactive oxygen species (ROS)

#### 3.5.1. Analysis of reactive oxygen species

To verify the catalytic mechanism of r-MIL-88A, ESR tests were tested with DMPO as a spin-trapping agent. Fig. S4 shows the ESR spectra of r-MIL-88A-H<sub>2</sub>O<sub>2</sub>-DMPO mixture and H<sub>2</sub>O<sub>2</sub>-DMPO mixture. The four-fold peaks consisted of a quartet with intensity ratios 1:2:2:1 with hyperfine coupling  $\alpha_{\text{N}} = \alpha_{\text{H}} = 14.9$  G that appeared in the curve of r-MIL-88A-H<sub>2</sub>O<sub>2</sub>-DMPO mixture, which is the characteristic signal of DMPO-·OH adduct [60]. In contrast, the ESR curve of the H<sub>2</sub>O<sub>2</sub>-DMPO mixture does not show the significant characteristic peaks of DMPO-·OH adduct, indicating that the importance of r-MIL-88A catalyst in generating hydroxyl radicals. In order further confirmed this results, 0.1 g of Benzoquinone, and *t*-butanol were added as scavenging species of ·OH and  $\cdot\text{O}_2^-$ , respectively [39]. As seen in Fig. 5B, the Fenton-like removal of phenol was inhibited obviously by *t*-butanol. Consequently, ·OH played a determined role for the phenol degradation in the r-MIL-88A reaction system.

Using terephthalic acid (TA) and 4-Chloro-7-nitrobenz-2-oxa-1,3-diazole (NBD-Cl) as probes, a fluorescence method could quantify the concentration of ·OH and  $\cdot\text{O}_2^-$ , respectively [39]. As shown in Fig. 7, for three kinds of MIL-88A-Fe, the fluorescence emission increases with increasing time for all of the samples. The shapes has greatly effluence for the formation of ·OH. The ability of producing ·OH has the order of r-MIL-88A > s-MIL-88A > d-MIL-88A, and the largest number of fluorescence emission spectra of r-MIL-88A is 428 a.u. in 30 min, which is larger than that of that of BiVO<sub>4</sub> composites (375 a.u.) [39]. In addition, the production of  $\cdot\text{O}_2^-$  was as much as 1/3 lower than that of ·OH from the concentration (Fig. 8). This result shows that ·OH is main ROS, and is consistent with published works [39,61].

#### 3.5.2. DFT caculation: H<sub>2</sub>O<sub>2</sub> dissociated energy barrier of (100) and (101) surface

DFT calculation was used to compare the H<sub>2</sub>O<sub>2</sub> activated ability on MIL-88A surface (100) and (101), and probe the H<sub>2</sub>O<sub>2</sub> dissociated process. As shown in Fig. 9A, B, for MIL-88A surface (100), the H<sub>2</sub>O<sub>2</sub> cleavage by O–O bond leads to the formation of ·OH has a low energy barrier of 0.58 eV, which is lower than that of cleavage into  $\cdot\text{O}_2^-$  (0.86 eV) when the cleavage of H–O bond. Both of pathways are exothermic. Compared with (100) surface, the (101) surface are hard to perform O–O bond cleavage, and its activation energy of the reaction is

0.84 eV, but this process is endothermic (Fig. 9C). Thus, ·OH suggested to be more easily formed on MIL-88A-Fe in Fenton-like reaction.

Our DFT calculation, confirmed two results: (1) the ·OH rather than  $\cdot\text{O}_2^-$ , is the main ROS; (2) H<sub>2</sub>O<sub>2</sub> dissociated energy barrier over MIL-88A surface (100) is low than that of (101). It can be concluded that the degradation performance of MIL-88A-Fe intensely relied on the surface architecture and the reactivity trend is in the order of (100) > (101) surface.

### 3.6. Structure-performance relationship

Aims to further analysis the structure-performance relationship. The total phenol removal efficiency could evaluate by TOF value [21], which could obtained by considering the number of degraded phenol molecules per Fe ions in the required time to 50% phenol degradation. The exposed Fe surface species can be quantified by XPS [21]. In this work, the surface iron content for r-, s- and d-MIL-88A-Fe are 16.5 wt%, 14.5 wt% and 12.3 wt% by XPS analysis, respectively. TOF could be obtained by weight of removal phenol (50%)/Fe element weight/the time of phenol degradation 50% [21]. The TOF value for three kinds of MIL-88A-Fe are about 5.0, 3.3 and 2.5 h<sup>-1</sup>, respectively. r-MIL-88A catalyst presented the highest TOF value (5.0 h<sup>-1</sup>), its activity also is better than  $\text{Fe}^{\text{II}}@\text{MIL-101(Fe)}$  (TOF = 1.2 h<sup>-1</sup>) and MIL-101(Fe) (TOF = 0.14 h<sup>-1</sup>) [21]. r-MIL-88A-Fe showed the highest TOF value, suggesting that it favored Fenton-like ability.

As shown in Fig. 10, their TOF value or reaction rate *k* value (from Fig. 4B), was correlated with the ratio of (100). It is seen that a linear-like relationship is obtained, revealing the (100) surface of MIL-88A-Fe to its activity well positively, and this surface determines its Fenton-like activity.

### 3.7. Spent catalysts

We also studied the XRD patterns, SEM image and XPS patterns of r-MIL-88-A before and after the reaction. Results showed the XRD patterns (Fig. S5), SEM picture (Fig. S6) and XPS survey (Fig. S7) results of r-MIL-88-A before and after catalytic process were almost the same, suggesting that the crystal structure of r-MIL-88-A was very stable during the oxidation process. In addition, the leaching metal ions from r-MIL-88-A particles were studied. In this work, the Fe ions in the solution after reaction has not been detected. No metal ions leaching suggests this catalyst could be used as highly active and stable heterogeneous catalysts for the Fenton-like process.

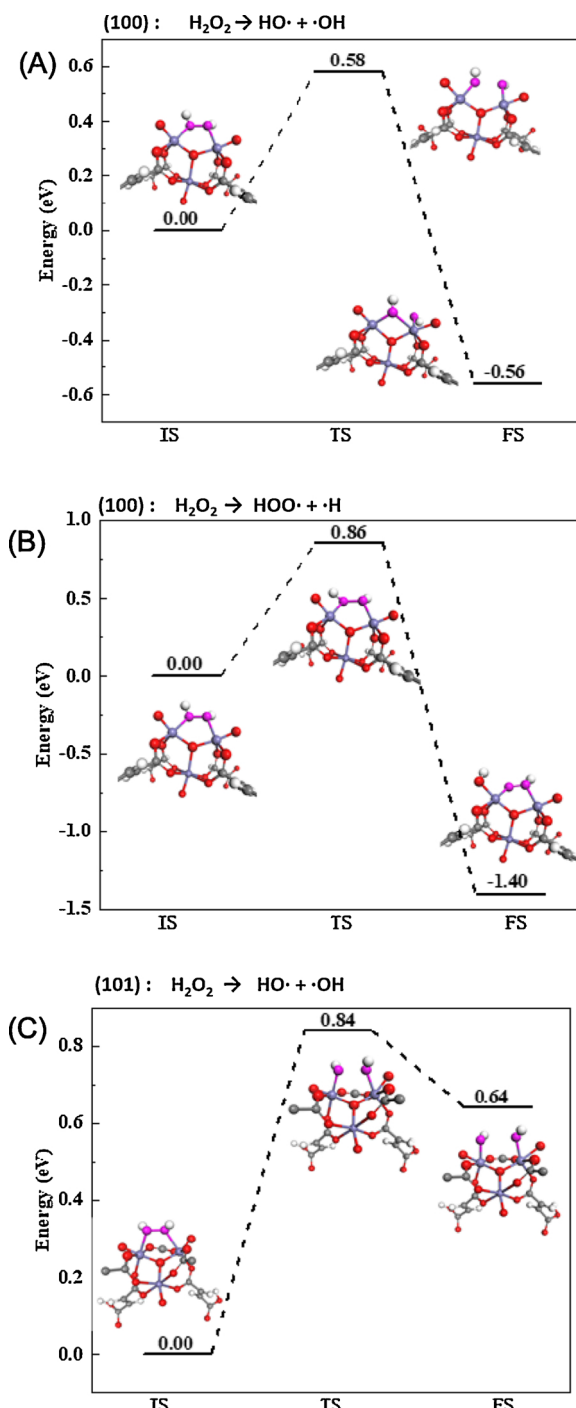


**Fig. 9.** Illustration of  $\text{H}_2\text{O}_2$  dissociated process over MIL-88A-Fe: (A) MIL-88A-Fe (100)  $\text{H}_2\text{O}_2 \rightarrow \text{HO}^\cdot + \cdot\text{OH}$ ; (B) MIL-88A-Fe (100)  $\text{H}_2\text{O}_2 \rightarrow \text{HOO}^\cdot + \cdot\text{H}$ ; (C) MIL-88A-Fe (101)  $\text{H}_2\text{O}_2 \rightarrow \text{HO}^\cdot + \cdot\text{OH}$ .

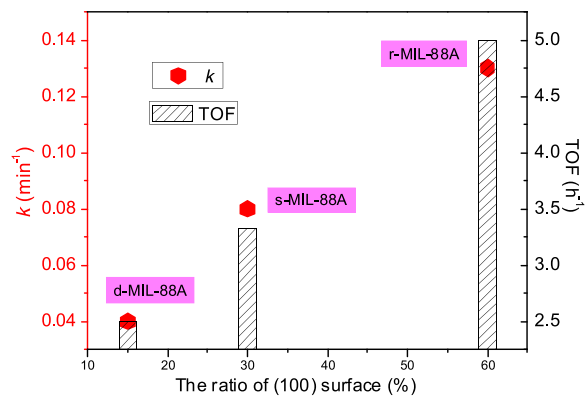
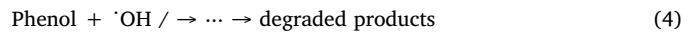
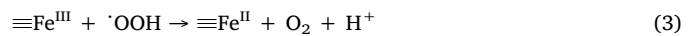
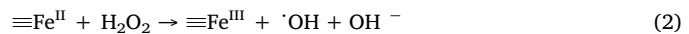
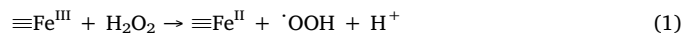


**Fig. 10.** Structure-performance relationship.

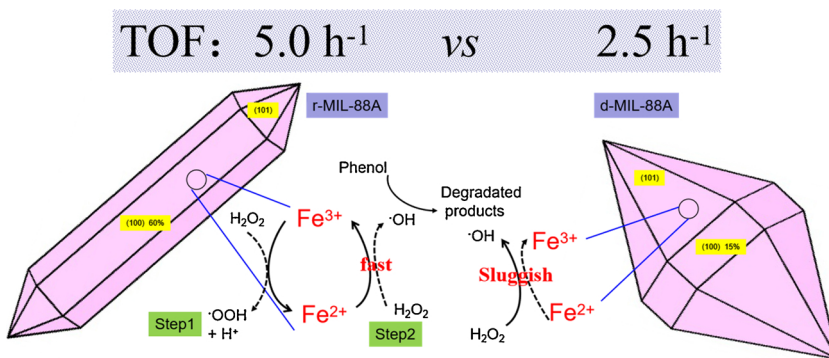
### 3.8. Reaction mechanism



For Fenton-like reaction over r-MIL-88A are demonstrated in **Scheme 2** and Eq.1–4. Two primary steps can be involved: for direct Fenton-like excitation of  $\text{H}_2\text{O}_2$ ,  $\text{H}_2\text{O}_2$  attacks  $\text{Fe}^{\text{III}}$  in r-MIL-88A to produce  $\text{Fe}^{\text{II}}$  (Eq.1), which further activates  $\text{H}_2\text{O}_2$  through Fenton-like reaction to generate  $\cdot\text{OH}$  radicals (Eq.2).  $\text{Fe}^{\text{II}}$  could be recovered from  $\text{Fe}^{\text{III}}$  by Eq. 3. A cyclic loop is formed and performs pollutants degradation (Eq.4). It should be noticed that the r-MIL-88A (100) surface possess low reaction energy barrier for generating  $\cdot\text{OH}$  as confirmed by DFT method. The more exposed (100) surface of r-MIL-88A is to enhance  $\text{H}_2\text{O}_2$  absorption and promote its dissociated intermediates. On the contrary, the s-MIL-88A and d-MIL-88A both perform lower activity because they possess less amount of (100) surfaces (**Scheme 2**).

### 4. Conclusions

The findings of this study reveals that r-MIL-88A with preferentially exposed (100) facets (60%), has excellent Fenton-like performance toward phenol removal, and phenol could be removed 100% in 15 min by the help of  $\text{H}_2\text{O}_2$  at room conditions. The performance of shaped MIL-88A-Fe material, has the order of r-MIL-88A (TOF  $5.0 \text{ h}^{-1}$ ) > s-MIL-88A (TOF  $3.3 \text{ h}^{-1}$ ) > d-MIL-88A (TOF  $2.5 \text{ h}^{-1}$ ). r-MIL-88A performs better Fenton-like activity than that of reported Fe-based MOFs, such as MIL-88B-Fe, MIL-101-Fe, and MIL-53(Fe) etc. DFT calculation shows that the  $\text{H}_2\text{O}_2$  activated behavior of r-MIL-88A (100) is easier than that of its (101) surface, it suggests that the r-MIL-88A can be used as an efficient and stable catalyst for Fenton-like reaction. To the best of our knowledge, this is the first report to investigate the Fenton-like behavior on a well-defined shape-controlled MIL-88A-Fe material by synergism of experimental and computational (DFT) study.



Scheme 2. Illustration of Fenton-like process over r-MIL-88A.

### Declaration of Competing Interest

The authors declare that they have no known competing financial interests or personal relationships that could have appeared to influence the work reported in this paper.

### Acknowledgements

This work was supported by the Project from the Tianjin Education Commission (2018KJ108 and 2018KJ111), National Key R&D Program of China (No.:2018YFC1902100), National Natural Science Foundation of China (No.31700516 and 21872125), and Foundation of Tianjin Key Laboratory of Pulp & Paper (No.201807). X. Liao would like to thank Shiyanjia Lab ([www.shyan.jia.com](http://www.shyan.jia.com)) for ESR test.

### Appendix A. Supplementary data

Supplementary material related to this article can be found, in the online version, at doi:<https://doi.org/10.1016/j.apcatb.2019.118064>.

### References

- [1] M. Cheng, C. Lai, Y. Liu, G. Zeng, D. Huang, C. Zhang, L. Qin, L. Hu, C. Zhou, W. Xiong, *Coord. Chem. Rev.* 359 (2018) 80–101.
- [2] J.L. Wang, L.J. Xu, *Appl. Catal. B Environ.* 123 (2012) 117–126.
- [3] M. Munoz, Z.M. de Pedro, J.A. Casas, J.J. Rodriguez, *Appl. Catal. B Environ.* 176 (2015) 249–265.
- [4] Y. Yao, H. Chen, C. Lian, F. Wei, D. Zhang, G. Wu, B. Chen, S. Wang, *J. Hazard. Mater.* 314 (2016) 129–139.
- [5] J. Tang, J. Wang, *Environ. Sci. Technol.* 52 (2018) 5367–5377.
- [6] X. Zhang, Y. Yang, L. Song, J. Chen, Y. Yang, Y. Wang, *J. Hazard. Mater.* 365 (2019) 597–605.
- [7] X. Zhang, Y. Yang, X. Lv, Y. Wang, N. Liu, D. Chen, L. Cui, *J. Hazard. Mater.* 366 (2019) 140–150.
- [8] X. Zhang, X. Lv, X. Shi, Y. Yang, Y. Yang, *J. Coll. Inter. Sci.* 539 (2019) 152–160.
- [9] X. Zhang, Y. Yang, W. Huang, Y. Yang, Y. Wang, C. He, N. Liu, M. Wu, L. Tang, *Mater. Res. Bull.* 99 (2018) 349–358.
- [10] W. Huang, N. Liu, X. Zhang, M. Wu, L. Tang, *Appl. Surf. Sci.* 425 (2017) 107–116.
- [11] N. Liu, C. Jing, Z. Li, W. Huang, B. Gao, F. You, X. Zhang, *Mater. Lett.* 237 (2019) 92–95.
- [12] H. Tian, T. Araya, R. Li, Y. Fang, Y. Huang, *Appl. Catal. B Environ.* 254 (2019) 371–379.
- [13] D. Wang, R. Huang, W. Liu, D. Sun, Z. Li, *ACS Catal.* 4 (2014) 4254–4260.
- [14] D. Wang, Y. Fang, W. Dong, G. Zeng, X. Li, Q. Yang, X. Yuan, *J. Coll. Inter. Sci.* 519 (2018) 273–284.
- [15] G. Liao, Y. Gong, L. Zhang, H. Gao, G. Yang, B. Fang, *Energy Environ. Sci.* 12 (2019) 2080–2147.
- [16] X. Zhang, X. Zhang, L. Song, F. Hou, Y. Yang, Y. Wang, N. Liu, *Inter. J. Hyd. Energy* 43 (2018) 18279–18288.
- [17] Y. Yang, H. Dong, Y. Wang, C. He, Y. Wang, X. Zhang, *J. Solid State Chem.* 258 (2018) 582–587.
- [18] X. Zhang, Y. Yang, L. Song, Y. Wang, C. He, Z. Wang, L. Cui, *Molecular Catal.* 447 (2018) 80–89.
- [19] X. Liu, Y. Zhou, J. Zhang, L. Tang, L. Luo, G. Zeng, *ACS Appl. Mater. Interfaces* 9 (2017) 20255–20275.
- [20] C. Gao, S. Chen, X. Quan, H. Yu, Y. Zhang, *J. Catal.* 356 (2017) 125–132.
- [21] H. Lv, H. Zhao, T. Cao, L. Qian, Y. Wang, G. Zhao, *J. Mol. Catal. A Mater. Chem.* 400 (2015) 81–89.
- [22] E.M. Dias, C. Petit, *J. Mater. Chem. A Mater. Energy Sustain.* 3 (2015) 22484–22506.
- [23] D. Yu, M. Wu, Q. Hu, L. Wang, C. Lv, L. Zhang, *J. Hazard. Mater.* 367 (2019) 456–464.
- [24] W.-T. Xu, L. Ma, F. Ke, F.-M. Peng, G.-S. Xu, Y.-H. Shen, J.-F. Zhu, L.-G. Qiu, Y.-P. Yuan, *Dalton Trans.* 43 (2015) 3792–3798.
- [25] N. Liu, W. Huang, X. Zhang, L. Tang, L. Wang, Y. Wang, M. Wu, *Chem. Eng. J.* 349 (2018) 603–612.
- [26] J. Amaro-Gahete, R. Klee, D. Esquivel, J. RafaelRuiz, C. Jiménez-Sanchidrián, F.J. Romero-Salgueiro, *Ultrason. Sonochem.* 50 (2019) 59–66.
- [27] C. Mellot-Draznieks, C. Serre, S. Surble, N. Audebrand, G. Férey, *J. Am. Chem. Soc.* 127 (2005) 16273–16278.
- [28] T. Chalati, P. Horcajada, R. Gref, P. Couvreur, C. Serre, *J. Mater. Chem.* 21 (2011) 2220–2227.
- [29] N. Liu, W. Huang, X. Zhang, L. Tang, L. Wang, Y. Wang, M. Wu, *Appl. Catal. B: Environ.* 221 (2018) 119–128.
- [30] D. Yu, L. Li, M. Wu, J.C. Crittenden, *Appl. Catal. B Environ.* 251 (2019) 66–75.
- [31] S.G. Khasevani, M.R. Gholami, *Inorg. Chem. Commun.* 102 (2019) 221–228.
- [32] Z. Zhao, D. Zhang, H. Li, C. Su, X. Pu, Y. Geng, *Sep. Purif. Technol.* 220 (2019) 16–24.
- [33] Y. Xue, S. Zheng, H. Xue, H. Pang, *J. Mater. Chem. A Mater. Energy Sustain.* 7 (2019) 7301–7327.
- [34] J. Liu, X. Li, B. Liu, C. Zhao, Z. Kuang, R. Hu, B. Liu, Z. Ao, J. Wang, *ACS Appl. Mater. Interfaces* 10 (2018) 38051–38056.
- [35] M. Ma, A. Betard, I. Weber, N.S. Al-Hokbany, R.A. Fischer, N. Metzler-Nolte, *Cryst. Eng. Comm.* 13 (2013) 2286–2291.
- [36] Z. Hasan, S.H. Jhung, *J. Hazard. Mater.* 283 (2015) 329–339.
- [37] H. Zhang, W. Wang, H. Zhao, L. Zhao, L. Zhao, L.Y. Gan, L.H. Guo, *ACS Catal.* 8 (2018) 9399–9407.
- [38] C. Zeng, X. Zhang, S. Hu, F. Chen, *Appl. Catal. B: Environ.* 216 (2017) 106–113.
- [39] T. Xu, R. Zhu, G. Zhu, J. Zhu, X. Liang, Y. Zhu, H. He, *Appl. Catal. B: Environ.* 212 (2017) 50–58.
- [40] X. Liao, Z. Hu, L. Ma, Q. Hao, S. Lu, *Chem. Eng. J.* 351 (2018) 280–294.
- [41] K.Y.A. Lin, H.A. Chang, C.J. Hsu, *RSC Adv.* 5 (2015) 32520–32530.
- [42] H. Guo, Y. Zhu, S. Wang, S. Su, L. Zhou, H. Zhang, *Chem. Mater.* 24 (2012) 444–450.
- [43] B. Shan, J.B. James, M.R. Armstrong, E.C. Close, P.A. Letham, K. Nikkhah, Y.S. Lin, B. Mu, *J. Phys. Chem. C* 122 (2018) 2200–2206.
- [44] L. Wang, Y. Zhang, X. Li, Y. Xie, J. He, J. Yu, Y. Song, *Sci. Rep.* 5 (2015) 14341.
- [45] X. Zhang, H. Li, X. Lv, J. Xu, Y. Wang, C. He, N. Liu, Y. Yang, Y. Wang, *Chemistry-A European J.* 24 (2018) 8822–8832.
- [46] X. Zhang, H. Li, F. Hou, Y. Yang, H. Dong, N. Liu, Y. Wang, L. Cui, *Appl. Surf. Sci.* 411 (2017) 27–33.
- [47] X. Zhang, F. Hou, Y. Yang, Y. Wang, N. Liu, D. Chen, Y. Yang, *Appl. Surf. Sci.* 423 (2017) 771–779.
- [48] Y. Guo, P. Wang, J. Qian, Y. Ao, C. Wang, J. Hou, *Appl. Catal. B: Environ.* 234 (2018) 90–99.
- [49] Q. Sun, M. Liu, K. Li, Y. Han, Y. Zuo, J. Wang, C. Song, G. Zhang, X. Guo, *Cryst. Eng. Comm.* 17 (2015) 7160–7168.
- [50] Q. Sun, M. Liu, K. Li, Y. Han, Y. Zuo, J. Wang, C. Song, G. Zhang, X. Guo, *Dalton Trans.* 45 (2016) 7952–7959.
- [51] W. Cui, J.Y. Li, W.L. Cen, Y.J. Sun, S.C. Lee, F. Dong, *J. Catal.* 352 (2017) 351–360.
- [52] X.W. Li, W.D. Zhang, W. Cui, Y.J. Sun, G.M. Jiang, Y.X. Zhang, H.W. Huang, F. Dong, *Appl. Catal. B: Environ.* 221 (2018) 482–489.
- [53] N. Liu, W. Huang, M. Tang, Y. C, B. Gao, Z. Li, L. Tang, J. Lei, L. Cui, X. Zhang, *Chem. Eng. J.* 359 (2019) 254–264.
- [54] X.D. Zhang, F.L. Hou, H.X. Li, Y. Yang, Y.X. Wang, N. Liu, Y.Q. Yang, *Microporous*

- Mesoporous Mater. 259 (2018) 211–219.
- [55] Y. Feng, L. Ling, J. Nie, K. Han, X. Chen, Z. Bian, H. Li, Z.L. Wang, ACS Nano 11 (2017) 12411–12418.
- [56] X.A. Dong, W.D. Zhang, Y.J. Sun, J.Y. Li, W.L. Cen, Z.H. Cui, H.W. Huang, F. Dong, J. Catal. 357 (2018) 41–50.
- [57] P.S. Johnson, P.L. Cook, X. Liu, W. Yang, Y. Bai, N.L. Abbott, F.J. Himpel, J. Chem. Phys. 135 (2011) 044702–044711.
- [58] Y. Li, J. Jiang, Y. Fang, Z. Cao, D. Chen, N. Li, Q. Xu, J. Lu, ACS Sustainable Chem. Eng. 6 (2018) 16186–16197.
- [59] X. Li, Y. Pi, L. Wu, Q. Xia, J. Wu, Z. Li, J. Xiao, Appl. Catal. B: Environ. 202 (2017) 653–663.
- [60] D. Wang, M. Wang, Z. Li, ACS Catal. 5 (2015) 6852–6857.
- [61] Y. Gao, Y. Wang, H. Zhang, Appl. Catal. B: Environ. 178 (2015) 29–36.